Research article

Kirill V. Voronin, Unai Aseguinolaza Aguirreche, Rainer Hillenbrand, Valentyn S. Volkov, Pablo Alonso-González and Alexey Y. Nikitin*

Nanofocusing of acoustic graphene plasmon polaritons for enhancing mid-infrared molecular fingerprints

https://doi.org/10.1515/nanoph-2020-0164
Received March 4, 2020; accepted April 24, 2020

Abstract: Mid-infrared (mid-IR) optical spectroscopy of molecules is of large interest in physics, chemistry, and biology. However, probing nanometric volumes of molecules is challenging because of the strong mismatch of their mid-infrared absorption and scattering cross-sections with the free-space wavelength. We suggest overcoming this difficulty by nanofocusing acoustic graphene plasmon polaritons (AGPs) – oscillations of Dirac charge carriers coupled to electromagnetic fields with extremely small wavelengths – using a taper formed by a graphene sheet above a metallic surface. We demonstrate that due to the appreciable field enhancement and mode volume reduction, the nanofocused AGPs can efficiently sense molecular fingerprints in nanometric volumes. We illustrate a possible realistic sensing scenario based on AGP interferometry performed with a near-field microscope. Our results can open new avenues for designing tiny sensors based on graphene and other 2D polaritonic materials.

Keywords: graphene plasmon; molecular sensing; nanofocusing.

***Corresponding author: Alexey Y. Nikitin**, Donostia International Physics Center (DIPC), Donostia-San Sebastian, 20018, Spain; and IKERBASQUE-Basque Foundation for Science, Bilbao, 48013, Spain, E-mail: alexey@dipc.org. https://orcid.org/0000-0002-2327-0164
Kirill V. Voronin: Center for Photonics and 2D Materials, Moscow Institute of Physics and Technology, Dolgoprudny, 141700, Russia; Skolkovo Institute of Science and Technology, Moscow, 121205, Russia. https://orcid.org/0000-0002-8911-1166
Unai Aseguinolaza Aguirreche: Centro de Fisica de Materiales CFM, CSIC-UPV/EHU, Donostia-San Sebastian, 20018, Spain; Donostia International Physics Center (DIPC), Donostia-San Sebastian, 20018, Spain; and Fisika Aplikatua 1 Saila, Gipuzkoako Ingenieritza Eskola, University of the Basque Country (UPV/EHU), Donostia-San Sebastian, 20018, Spain
Rainer Hillenbrand: CIC nanoGUNE BRTA and Department of Electricity and Electronics, UPV/EHU, Donostia-San Sebastian, 20018, Spain; IKERBASQUE-Basque Foundation for Science, Bilbao, 48011, Spain
Valentyn S. Volkov: Center for Photonics and 2D Materials, Moscow Institute of Physics and Technology, Dolgoprudny, 141700, Russia
Pablo Alonso-González: Department of Physics, University of Oviedo, Oviedo, 33006, Spain; Center of Research on Nanomaterials and Nanotechnology, CINN (CSIC–Universidad de Oviedo), El Entrego, 33940, Spain

1 Introduction

Nondestructive analysis of molecules by means of mid-infrared (mid-IR) spectroscopy is of high relevance for plenty of vital applications in organic and inorganic chemistry, particularly for gas concentration control, identification of polymer degradation, or determining the blood alcohol content, to name a few. The molecule of interest is typically recognized *via* its vibrational fingerprint in extinction spectra [1, 2]. In conventional spectroscopic experiments, the sample is illuminated by an incident wave of different frequencies, and the transmitted or reflected light is captured by a detector. This simple technique, however, does not allow for studying small amounts of molecules in nanometric volumes as the cross-section of the latter is much smaller than the wavelength of light, and thus the absorption or scattering signals are too small to be detected. This difficulty can be partially overcome by exciting surface plasmon polaritons (SPPs) – collective oscillations of free charge carriers coupled to an electromagnetic field – on the surface of a conductor. Due to the field confinement and enhancement that SPPs provide, the scattering and absorption cross-section of the molecular volumes can be enlarged and the signals detected greatly enhanced. For instance, by exciting localized SPPs in mid-IR optical antennas covered by a layer of molecules, it is possible to significantly increase the infrared response of the molecular layer, which is the basis for the well-established surface-enhanced infrared spectroscopy (SEIRA) [3–5]. Nevertheless, at mid-IR frequencies, the confinement of

SPPs on metal surfaces and simple dipole antennas is not as strong as in the visible range, such that sensing of nanometric volumes of molecules is challenging, unless one uses narrow-gap antennas [6, 7] or SPP dimers [8–10]. The optical response of these metallic structures is, however, difficult to control in an active manner (e.g., by applying a voltage) and thus cannot be efficiently tuned through a broad spectral interval.

Unlike metals, graphene supports plasmon polaritons (GPs) with much larger wavevectors, and as a consequence, much stronger vertical field confinement [11]. Moreover, being compatible with complementary metal–oxide–semiconductor (CMOS) platforms, graphene-based sensing components potentially allow for their on-chip integration [12]. Importantly, GPs can also be actively tuned by varying the Fermi level in graphene and thus the number of charge carriers on it (such tuning can be made by simply applying an external voltage *via* back-gating). In addition, graphene shows a high nonlinearity of its optical response [13, 14]. All these properties make graphene an outstanding candidate for developing an ample range of optoelectronic devices [13, 15]. The latter advantage has recently been applied in an SEIRA-like bio-sensor consisting of an array of resonant graphene ribbons covered by a polymer film [16]. An alternative to molecular spectroscopy based on SEIRA could consist of analyzing the near-field properties of propagating GPs when they interact with a nanometric-thin molecular layer on top of the graphene sheet [17]. Such interaction, if governed by absorption, is expected to produce strong effects in the amplitude and phase of the GPs as well as in their wavelength, which can be directly related to the molecules absorption fingerprints. To increase the sensitivity of such polaritonic sensing platform, one can explore the use of electromagnetically screened GPs, also known as "acoustic" GPs (AGPs), supported by a graphene sheet placed above a metallic pad [18–22] (far-field SEIRA-like sensing with AGP nanoresonators has been suggested in [23] and later on demonstrated experimentally in [24]), which are known to show a very strong field confinement and a linear dispersion. To further increase the field confinement of AGPs and thus couple more efficiently to the molecules vibrations, one can make use of a nanofocusing concept [25]. The latter consists of the propagation of an electromagnetic mode along a tapered waveguide so that both its cross-section and wavelength gradually reduce, leading to a dramatic increase of the electromagnetic field intensity at the taper apex [26, 27]. Although this nanofocusing concept has been reported for AGPs (particularly, to study the deceleration of the AGPs) [28], its application for molecular sensing has not yet been explored.

Here we introduce the concept of mid-IR molecular spectroscopy with nanofocused AGPs as follows: by gradually reducing the spacer layer between graphene and a metallic pad (a typical architecture for graphene-based nanodevices), GPs adiabatically convert into (much stronger confined) AGPs, without any need of momentum matching; then, AGPs propagate towards a minute volume of molecules and reflects back from the sharp region of the taper. The molecular fingerprint is encoded into the AGPs propagating properties (the amplitude, phase and wavelength), which can be probed by the tip of a near-field microscope.

2 Acoustic graphene plasmon polaritons

We first briefly characterize the properties of AGPs. Figure 1A shows the dispersion of AGP in the frequency range of 500–2000 cm^{-1} for different values of the spacer layer, d, (from 150 to 3 nm) at a typical Fermi level E_f = 0.44 eV, assuming the propagation along the x-axis. Since we do not stick to any particular experiment, we assume a transparent spacer layer (as, for instance, CaF_2) with a dielectric permittivity equal to 1. On the other hand, from Eq. (8) of the Supplementary Material, it follows that considering the dielectric permittivity ε different from 1, is equivalent to rescaling the spacer thickness as $d \to d/\varepsilon$. For sufficiently large d (green and cyan curves), the dispersion of AGPs scales similarly to GPs (black curve), i. e., $\omega \propto \sqrt{k_x}$, due to the weak field screening by the metallic substrate. As soon as the confinement length of GPs, given by $2\pi/k_x$, becomes comparable to d, the field screening becomes important and GPs hybridizes with its mirror image in the metal region giving rise to an AGP mode [18]. In contrast to GPs, the dispersion of AGPs has a liner scaling with momentum and is strongly dependent upon d, $\omega \propto k_x\sqrt{d}$, so that with decreasing d the momentum of AGPs increases as well as their confinement and thus a major portion of the electromagnetic energy is flowing inside the spacer layer.

The Figure of Merit (FOM) of AGP defined as the propagation length L_p normalized to the AGP wavelength λ_p as a function of frequency ω is shown in Figure 1B. The damping (lifetime τ = 0.1 ps) is chosen to correspond to realistic graphene samples commonly used in optical experiments. In the shown frequency interval, FOM ranges from 2 to 5 for most of the values of d, which means that AGP can propagate several wavelengths along graphene. Interestingly, FOM has larger values for smaller d. This can be explained by a quicker reduction of λ_p (due to the

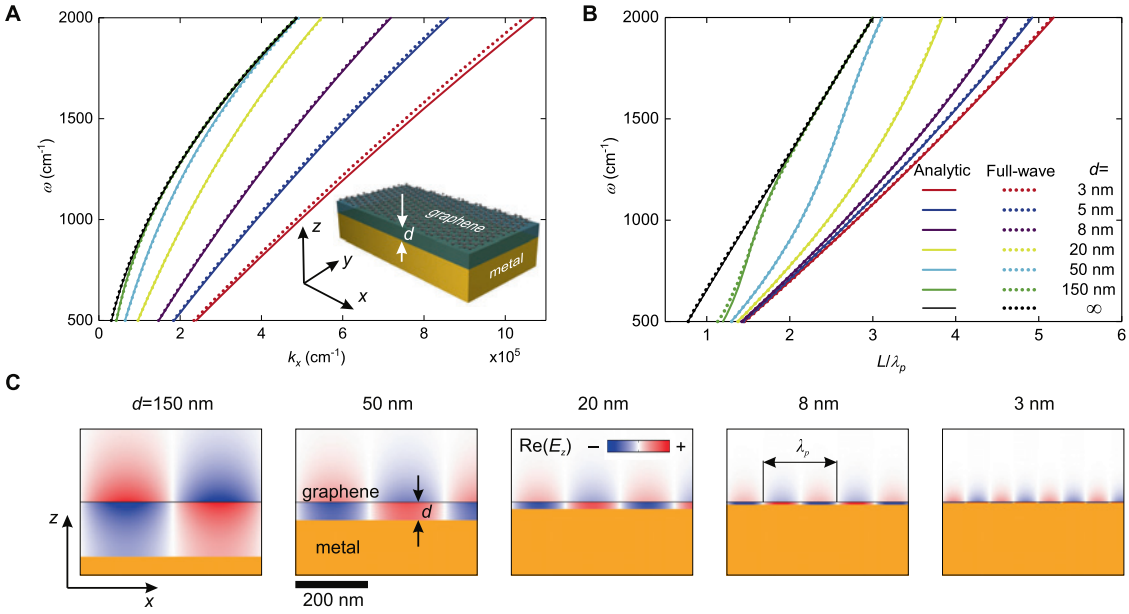

Figure 1: Properties of AGP. (A) AGPs dispersion for different thicknesses of the spacer layer, d. (B) The figure of Merit L_p/λ_p, of AGPs as a function of frequency for several values of d. (C) Spatial field distribution of AGPs, Re[$E_z(x,z)$], for $\omega = 1000$ cm^{-1} and several values of d. In all panels, we assume $E_F = 0.44$ eV and a lifetime $\tau = 0.1$ ps.

confinement increase), compared with L_p (due to the group velocity decrease). Analytical results for this same system, shown in Figures 1B and C by continuous curves (explained in more detail in the Supplementary Material) are in excellent agreement with full-wave simulations (Comsol), shown by dotted curves.

To demonstrate the AGPs field confinement, we show in Figure 1C the spatial distribution of their vertical electric field component. We observe that inside the spacer, at any fixed distance x, E_z is nearly independent upon the vertical coordinate, z, thus being similar to the electric field distribution inside a capacitor, which is a typical characteristic of an acoustic mode. Moreover, we can clearly see a reduction of the distance between field oscillations for smaller d, indicating a wavelength reduction of AGPs (due to a momentum increase). As can be expected from this field distribution and their dispersion relation, under gradual reduction of d along the propagation direction, the AGP wavelength should compress, while the energy flux increase for energy conservation reasons.

3 Nanofocusing of acoustic graphene plasmon polaritons

Consider an AGP traveling in the x-direction along a graphene sheet placed above a metal substrate. The separation distance d between graphene and metal gradually decreases, forming a taper, as shown in Figure 2A. We assume that far away from the taper apex (in the region, where the graphene-meal separation is significant) the AGP is similar to a conventional GP and the latter is excited by the standard methods, as, for example by a tip of a near-field microscope [29, 30]. In order to focus on the physics of the AGP compression, we can neglect the influence of the source (the tip) on the fields of the AGP. For the same reason, we do not consider the geometrical spreading factor (cylindrical wave decay) present in AGPs when excited by a localized source. Assuming the shallow angles of the taper (d slowly decreases with x on the scale of λ_p), the electric field of the AGP propagating along the taper can be found by the slowly varying envelope approximation (see Supplementary Material). Namely, the electric field of the AGP at any point can be written as:

$$E_z(x, z) = A(x)E_{AGP}(x, z)e^{i\Phi(x)}, \quad (1)$$

where $E_{AGP}(x, z)$ presents the mode profile of the AGP, $A(x)$ is the slowly varying amplitude, and $\Phi(x) = \int_0^x k_x(x')dx'$ is the accumulating phase (we assume that AGP is excited at $x = 0$). While $E_{AGP}(x, z)$ and k_x can be explicitly found from Maxwell's equations, by properly matching the electric and magnetic fields on the graphene sheet and metal surface, the amplitude $A(x)$ is determined by the energy flux conservation. Although such a method is very precise for the lossless case, it turns to provide a very good estimation for the electric field for our system with relatively small losses.

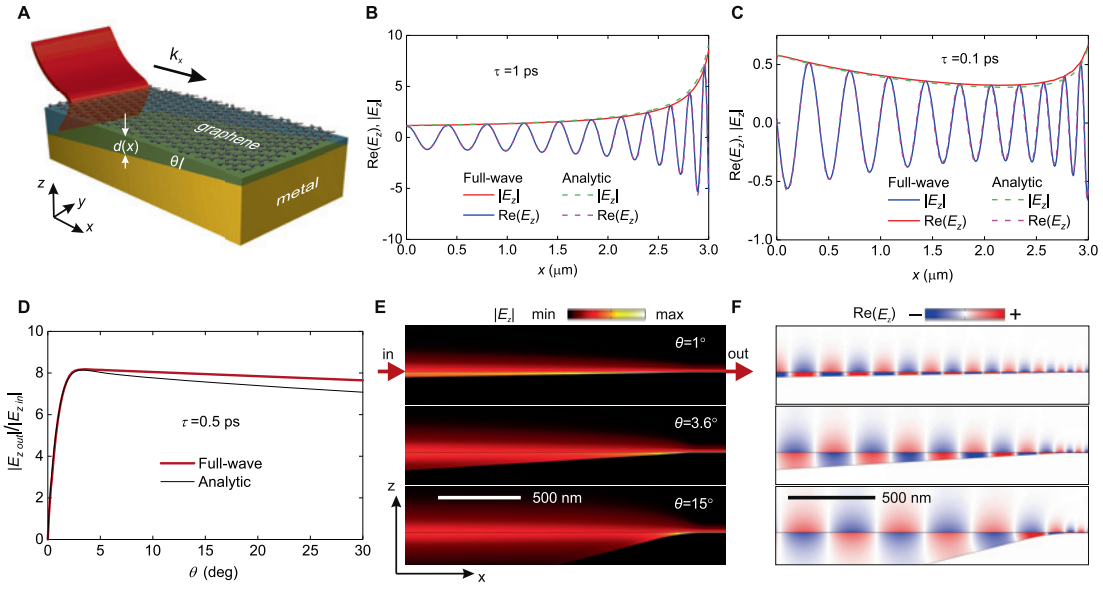

Figure 2: Nanofocusing of AGPs. (A) Schematics of the taper with the propagating AGP. (B, C) vertical field profiles, Re[$E_z(x, z)$] and $|E_z(x, z)|$ along with the graphene sheet ($z = -0.5$ nm) for two different values of τ. (D) Vertical field enhancement $|E_z(x, z)/E_{z\,in}|$ as a function of θ. (E) The absolute value of the vertical component of the AGP field $|E_z(x, z)|$ for different values of the tapering angle θ considering $\tau = 0.5$ ps. (F) Same as (E) for the real part, Re[$E_z(x, z)$]. In all panels we assume $E_F = 0.44$ eV and $\omega = 1000$ cm^{-1}.

Namely, for finite relaxation time, τ, the AGP wavevector k_x acquires the imaginary part and so $\Phi(x)$, which leads to the loss of energy by the AGP during the propagation.

The results of the full-wave simulations of the vertical electric field (continuous curves) of AGPs propagating along the taper together with those given by the analytical approximation in Eq. (1) (dashed curves) are illustrated in Figure 2B and C for two values of τ. In the simulations, we excite the AGPs at the left port of the domain ("in"), let it propagate through the taper, and then pass through the right port of the domain ("out") without back reflection. As observed, the analytical and numerical results are in excellent agreement, which confirms the validity of Eq. (1) (the highest deviation between the field calculated analytically and the result of the simulation is less than 7% for taper angles on the order of 1 degree), even though losses in graphene lead to breaking of the energy flux conservation, used to determine $A(x)$. In the field profiles, one can clearly see the simultaneous wavelength reduction ($\lambda_p \propto \sqrt{d}$) and the electric field enhancement (the amplitude of the electric field scales as $\propto d^{-3/4}$) both observations being the landmarks of the nanofocusing effect. Remarkably, while for larger values of τ (corresponding to high-quality graphene) the AGP field amplitude shows a monotonous increase (Figure 2B), for moderate τ, the exponential decay along x competes with nanofocusing and leads to the formation of a minimum at a certain position between the source and the taper end (Figure 2C). Figure 2D presents the field enhancement (ratio between the vertical electric field values at the ending and starting points of the taper) as a function of the tapering angle, θ. The field enhancement has an optimum at a small angle $\theta_{opt} = 3.6°$, after which it monotonically decreases with θ in the shown interval. This optimum angle corresponds to a balance between nanofocusing and absorption in the narrow region of the taper. In Figure 2E and F the spatial distribution of the electric field is represented for three values of the tapering angle: $\theta < \theta_{opt}$, $\theta = \theta_{opt}$, and $\theta > \theta_{opt}$. All the three cases show a nanofocusing effect, with a clear hot spot formation at the ending of the taper, which should be beneficial for the interaction of AGPs with molecular resonances.

4 Molecule fingerprint enhancement

We now illustrate a possible scenario for sensing molecules with AGPs, as well as the advantage of using nanofocused AGPs for this purpose. To that end, in the full-wave simulations, we continue the taper with a narrow graphene/spacer/metal channel of 2 nm in thickness and a finite length, w (the numerical simulations were performed for w values of 10, and 20 nm), as shown in Figure 3D. Then, we

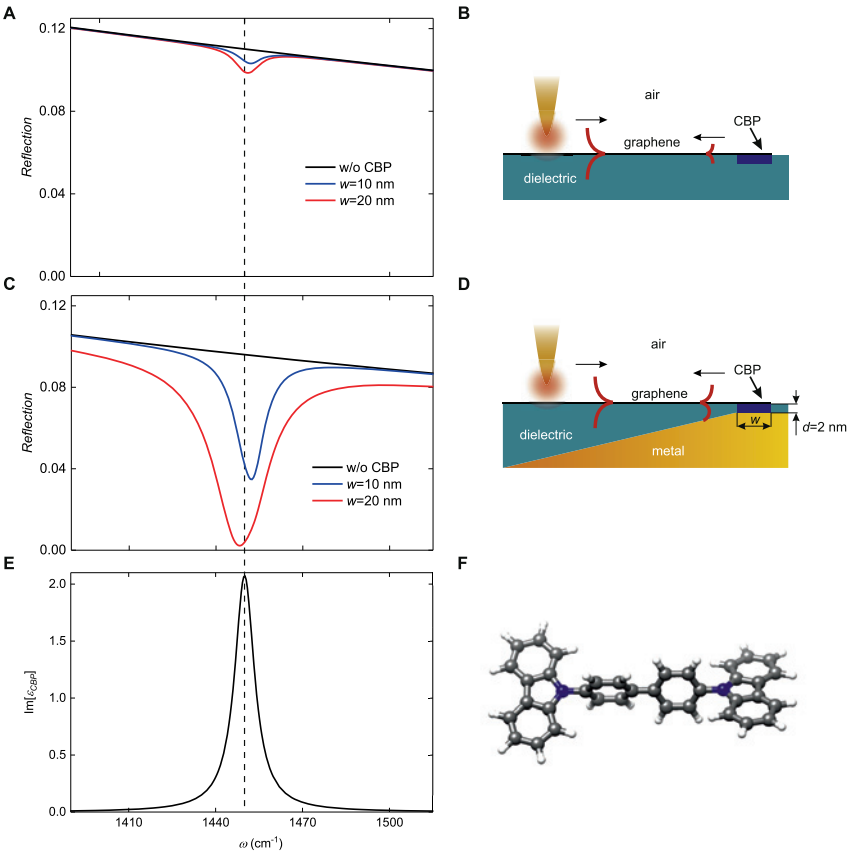

Figure 3: Probing the vibrational fingerprint of a molecule with a nanofocused AGP. (A) The reflection coefficient of a GP as a function of ω for two values of w. (B) Schematics of the sensing with GP. (C) Same as (A), for AGP. (D) Schematics of the sensing with AGP. (E) The spectral fingerprint of CBP molecules: $\mathrm{Im}(\varepsilon_{CBP})$ as a function of w. (F) Schematics of the CBP molecule atomic structure. In (A), (C), and (E), we assume $E_F = 0.44$ eV and $\tau = 0.5$ ps.

fill up the spacer with molecules and calculate the AGPs reflection from the end of the channel. Such simulation mimics a standard experiment with scattering-type scanning near-field microscope (s-SNOM), in which a polariton is launched and probed by a tip via polariton interferometry [29, 30]. For a proof of principle purpose, we consider CBP molecules, used in recent mid-IR polaritonic experiments [31], (see schematics in Figure 3F). We model its dielectric permittivity, ε_{CBP}, as a Drude-Lorentz oscillator, according to [31], so that $\mathrm{Im}(\varepsilon_{CBP})$ shows a sharp peak at $\omega = 1450$ cm^{-1} (Figure 3E), corresponding to one of the the CH deformation modes [32]. In Figure 3A we show the reflection of a conventional GP (without nanofocusing) from the molecular region (see the corresponding schematics in Figure 3B) as a function of ω. One can recognize the CBP fingerprint in the reflection spectrum, although its visibility (which we define as the maximal relative difference between the reflection coefficient amplitude with and without the molecules, normalized to the reflection coefficient amplitude without the molecules) is about 0.067 and 0.100 for $w = 10$ nm and $w = 20$ nm, respectively. In stark contrast, the same simulation with the nanofocused AGP yields much deeper reflection minima, matching the vibrational resonance of the CBP. More precisely, the fingerprint provided by AGP is about one order of magnitude larger than that provided by GP: the visibility is 0.63 and 0.98 for $w = 10$ nm and $w = 20$ nm, respectively. The dependence of the visibility of the fingerprint upon w (shown in Figure 1 of the Supplementary Material) also clearly demonstrates the much stronger accumulation of the absorption along with the layer for AGP with respect to GP. Let us note that the peaks in the spectrum of the plasmon polariton reflection coefficient (Figures 3A and B) are slightly broader than the peak of the CBP molecules. This broadening results from dissipation in graphene. Although the broadening of the molecular fingerprints will not impede the sensing of narrower vibrational resonances, it can negatively affect the resolution of closely located peaks, thus limiting the selectivity of the sensor.

Taking into account such strong sensitivity of AGP to the presence of the molecules, one can foresee that by properly matching the length of the molecular layer, strong coupling between AGPs and molecular vibrational modes can emerge. Namely, when an integer number of half-AGP wavelength, $\lambda_p/2$, fits along the length w, a Fabry–Perot resonance condition is fulfilled, with a resulting enhanced electromagnetic field that makes the vibrational resonance of the molecule split into two hybridized AGP-vibrational

modes, similarly to [31]. The detailed analysis of this interesting phenomenon, however, goes beyond the scope of the current manuscript. It is also worth noticing that due to the absence of cutoff in the AGP mode for any given spacer thickness, d, further reduction of d (together with the length of the probed region, w) can potentially enable coupling between AGPs and a few, (or even with a single) molecules. In this case, however, nonlocal effects will play a crucial role [6, 19, 20]. Namely, nonlocal effects manifest as a dependence of the graphene conductivity with the wavevector of AGPs, and typically appear when the group velocity of the plasmon becomes close to the Fermi velocity of electrons in graphene. Nonlocal effects prevent an increase in localization of the AGP field and a decrease in the plasmon wavelength for smaller gaps, which can lead to a limitation of the sensitivity. In our system, the nonlocal effects do not play a significant role, since the minimum slowest group velocity is $3.6{\cdot}10^6$ m/s, thus, exceeding for more than three times the Fermi velocity in graphene (10^6 m/s [33]).

5 Conclusion

We have suggested a method of probing molecular fingerprints with nanofocused AGPs. Moreover, we have shown that the nanofocusing of AGPs can be achieved in graphene with a moderate relaxation time of its charge carriers. Importantly, since AGPs modes do not have any cutoff, they can propagate inside arbitrary thin graphene-metal gaps (although at some point the propagation is limited by nonlocal quantum effects) and thus can be used to probe minute amounts of molecules. We have demonstrated that the visibility of molecular fingerprints by means of nanofocused AGPs is one order of magnitude higher than the visibility achieved with conventional GPs. We foresee that a similar sensing scenario can be also realized making use of photothermoelectric effects in graphene when the AGP power absorbed by the molecules could be measured electrically [18, 34]. Moreover, other 2D materials [35–37] can also be potentially used for polaritonic focusing and sensing based on the same principles here reported. Our findings could find interesting applications for on-chip sensing of an extremely small amount of molecules.

Acknowledgments: A.Y.N. acknowledges the Spanish Ministry of Science, Innovation and Universities (national project MAT2017-88358-C3-3-R). K.V.V. and V.S.V. acknowledge the Russian Science Foundation, grant number 18-79-10208. P.A-G. acknowledges support from the European Research Council under Starting Grant 715496, 2DNANOPTICA. R.H. acknowledges support from the Spanish Ministry of Economy, Industry, and Competitiveness (National Project RTI2018-094830-B-100 and the Project MDM-2016-0618 of the Marie de Maeztu Units of Excellence Program) and the Basque Government (Grant No. IT1164-19).

References

[1] P. Larkin, "Preface," in *Infrared and Raman Spectroscopy*, P. Larkin, Ed., Oxford, Elsevier, 2011, pp. ix-x.

[2] A. Wokaun, and B. Schrader, "Infrared and Raman spectroscopy - methods and applications," *Berichte der Bunsengesellschaft für physikalische Chemie*, vol. 100, pp. 1268, 1996, https://doi.org/10.1002/bbpc.19961000733.

[3] F. Neubrech, C. Huck, K. Weber, A. Pucci, and H. Giessen, "Surface-enhanced infrared spectroscopy using resonant nanoantennas," *Chem. Rev.*, vol. 117, pp. 5110–5145, 2017, https://doi.org/10.1021/acs.chemrev.6b00743.

[4] F. Neubrech, A. Pucci, T. W. Cornelius, S. Karim, A. García-Etxarri, and J. Aizpurua, "Resonant plasmonic and vibrational coupling in a tailored nanoantenna for infrared detection," *Phys. Rev. Lett.*, vol. 101, p. 157403, 2008, https://doi.org/10.1103/physrevlett.101.157403.

[5] A. Pucci, F. Neubrech, J. Aizpurua, T. Cornelius, and M. L. de la Chapelle, "Electromagnetic nanowire resonances for field-enhanced spectroscopy," in *One-Dimensional Nanostructures*, Z. M. Wang, Ed., New York, Springer, 2008, pp. 175–215.

[6] J. J. Baumberg, J. Aizpurua, M. H. Mikkelsen, and D. R. Smith, "Extreme nanophotonics from ultrathin metallic gaps," *Nature Mater.*, vol. 18, pp. 668–678, 2019, https://doi.org/10.1038/s41563-019-0290-y.

[7] L. Dong, X. Yang, C. Zhang, et al., "Nanogapped au antennas for ultrasensitive surface-enhanced infrared absorption spectroscopy," *Nano Lett.*, vol. 17, pp. 5768–5774, 2017, https://doi.org/10.1021/acs.nanolett.7b02736.

[8] K. L. Domina, V. V. Khardikov, V. Goryashko, and A. Y. Nikitin, "Bonding and antibonding modes in metal–dielectric–metal plasmonic antennas for dual-band applications," *Adv. Opt. Mater.*, vol. 1900942, 2019, https://doi.org/10.1002/adom.201900942.

[9] Y.-C. Chang, S.-M. Wang, H.-C. Chung, C.-B. Tseng, and S.-H. Chang, "Observation of absorption-dominated bonding dark plasmon mode from metal–insulator–metal nanodisk arrays fabricated by nanospherical-lens lithography," *ACS Nano*, vol. 6, pp. 3390–3396, 2012, https://doi.org/10.1021/nn300420x.

[10] I. Romero, J. Aizpurua, G. W. Bryant, and F. J. Gd. Abajo, "Plasmons in nearly touching metallic nanoparticles: singular response in the limit of touching dimers," *Opt. Express*, vol. 14, pp. 9988–9999, 2006, https://doi.org/10.1364/oe.14.009988.

[11] P. A. D. Gonçalves, and N. M. R. Peres, *An Introduction to Graphene Plasmonics*, Singapore, World Scientific, 2016.

[12] T.-C. Wu, A. De Luca, Q. Zhong, et al., "Inkjet-printed CMOS-integrated graphene–metal oxide sensors for breath analysis," *npj 2D Mater. Appl.*, vol. 3, p.42, 2019, https://doi.org/10.1038/s41699-019-0125-3.

[13] Q. Bao, H. Zhang, Z. Ni, et al., "Monolayer graphene as a saturable absorber in a mode-locked laser," *Nano Res.*, vol. 4, pp. 297–307, 2011, https://doi.org/10.1007/s12274-010-0082-9.
[14] H. Zhang, S. Virally, Q. Bao, et al., "Z-scan measurement of the nonlinear refractive index of graphene," *Opt. Lett.*, vol. 37, pp. 1856–1858, 2012, https://doi.org/10.1364/ol.37.001856.
[15] Q. Bao, H. Zhang, B. Wang, et al., "Broadband graphene polarizer," *Nature Photon.*, vol. 5, pp. 411–415, 2011, https://doi.org/10.1038/nphoton.2011.102.
[16] D. Rodrigo, O. Limaj, D. Janner, et al., "Mid-infrared plasmonic biosensing with graphene," *Science*, vol. 349, pp. 165–168, 2015, https://doi.org/10.1126/science.aab2051.
[17] Y. Francescato, V. Giannini, J. Yang, M. Huang, and S. A. Maier, "Graphene sandwiches as a platform for broadband molecular spectroscopy," *ACS Photon.*, vol. 1, pp. 437–443, 2014, https://doi.org/10.1021/ph5000117.
[18] P. Alonso-González, A. Y. Nikitin, Y. Gao, and et al., "Acoustic terahertz graphene plasmons revealed by photocurrent nanoscopy," *Nature Nanotechnol.*, vol. 12, pp. 31–35, 2017, https://doi.org/10.1038/nnano.2016.185.
[19] M. B. Lundeberg, Y. Gao, R. Asgari, et al., "Tuning quantum nonlocal effects in graphene plasmonics," *Science*, vol. 357, pp. 187–191, 2017, https://doi.org/10.1126/science.aan2735.
[20] D. Alcaraz Iranzo, S. Nanot, E. J. C. Dias, et al., "Probing the ultimate plasmon confinement limits with a van der Waals heterostructure," *Science*, vol. 360, pp. 291–295, 2018, https://doi.org/10.1126/science.aar8438.
[21] A. Principi, R. Asgari, and M. Polini, "Acoustic plasmons and composite hole-acoustic plasmon satellite bands in graphene on a metal gate," *Solid State Commun.*, vol. 151, pp. 1627–1630, 2011, https://doi.org/10.1016/j.ssc.2011.07.015.
[22] X. Gu, I. T. Lin, and J.-M. Liu, "Extremely confined terahertz surface plasmon-polaritons in graphene-metal structures," *Appl. Phys. Lett.*, vol. 103, p. 071103, 2013, https://doi.org/10.1063/1.4818660.
[23] S. Chen, M. Autore, J. Li, et al., "Acoustic graphene plasmon nanoresonators for field-enhanced infrared molecular spectroscopy," *ACS Photon.*, vol. 4, pp. 3089–3097, 2017, https://doi.org/10.1021/acsphotonics.7b00654.
[24] I.-H. Lee, D. Yoo, P. Avouris, T. Low, and S.-H. Oh, "Graphene acoustic plasmon resonator for ultrasensitive infrared spectroscopy," *Nature Nanotechnol.*, vol. 14, pp. 313–319, 2019, https://doi.org/10.1038/s41565-019-0363-8.
[25] M. I. Stockman, "Nanofocusing of optical energy in tapered plasmonic waveguides," *Phys. Rev. Lett.*, vol. 93, p. 137404, 2004, https://doi.org/10.1103/physrevlett.106.019901.
[26] A. Y. Nikitin, P. Alonso-González, and R. Hillenbrand, "Efficient coupling of light to graphene plasmons by compressing surface polaritons with tapered bulk materials," *Nano Lett.*, vol. 14, pp. 2896–2901, 2014, https://doi.org/10.1021/nl500943r.
[27] A. Y. Nikitin, E. Yoxall, M. Schnell, et al., "Nanofocusing of hyperbolic phonon polaritons in a tapered boron nitride slab," ACS Photon., vol. 3, pp. 924–929, 2016, https://doi.org/10.1021/acsphotonics.6b00186.
[28] M. Y. Morozov, and V. V. Popov, "Nanofocusing and deceleration of terahertz plasma waves in tapered metal-insulator-graphene heterostructure," *J. Phys. Condens. Matter*, vol. 31p. 34LT02, 2019, https://doi.org/10.1088/1361-648x/ab22e3.
[29] J. Chen, M. Badioli, P. Alonso-González, et al., "Optical nano-imaging of gate-tunable graphene plasmons," Nature, vol. 487, pp. 77–81, 2012, https://doi.org/10.1038/nature11254.
[30] Z. Fei, A. S. Rodin, G. O. Andreev, et al., "Gate-tuning of graphene plasmons revealed by infrared nano-imaging," *Nature*, vol. 487, pp. 82–85. 2012, https://doi.org/10.1038/nature11253.
[31] M. Autore, P. Li, I. Dolado, et al., "Boron nitride nanoresonators for phonon-enhanced molecular vibrational spectroscopy at the strong coupling limit," *Light Sci. Appl.*, vol. 7, p. 17172, 2018, https://doi.org/10.1038/lsa.2017.172.
[32] T. Glaser, S. Beck, B. Lunkenheimer, et al., "Infrared study of the MoO3 doping efficiency in 4,4′-bis(N-carbazolyl)-1,1′-biphenyl (CBP)," *Org. Electron.*, vol. 14, pp. 575–583, 2013, https://doi.org/10.1016/j.orgel.2012.11.031.
[33] A. H. Castro Neto, F. Guinea, N. M. R. Peres, K. S. Novoselov, and A. K. Geim, "The electronic properties of graphene," *Rev. Mod. Phys.*, vol. 81, pp. 109–162, 2009, https://doi.org/10.1103/revmodphys.81.109.
[34] M. B. Lundeberg, Y. Gao, A. Woessner, et al., "Thermoelectric detection and imaging of propagating graphene plasmons," *Nature Mat.*, vol. 16, pp. 204–207, 2017, https://doi.org/10.1038/nmat4755.
[35] Z. Xie, C. Xing, W. Huang, et al., "Ultrathin 2D nonlayered tellurium nanosheets: facile liquid-phase exfoliation, characterization, and photoresponse with high performance and enhanced stability," *Adv. Funct. Mater.*, vol. 28, p. 1705833, 2018, https://doi.org/10.1002/adfm.201705833.
[36] W. Huang, Z. Xie, T. Fan, et al., "Black-phosphorus-analogue tin monosulfide: an emerging optoelectronic two-dimensional material for high-performance photodetection with improved stability under ambient/harsh conditions," *J. Mater. Chem. C.*, vol. 6, pp. 9582–9593, 2018, https://doi.org/10.1039/c8tc03284j.
[37] Z. Xie, F. Zhang, Z. Liang, et al., "Revealing of the ultrafast third-order nonlinear optical response and enabled photonic application in two-dimensional tin sulfide," *Photon. Res.*, vol. 7, pp. 494–502, 2019, https://doi.org/10.1364/prj.7.000494.

Supplementary material: The online version of this article offers supplementary material (https://doi.org/10.1515/nanoph-2020-0164).